



Equilibrium sorption of fluoride on the activated alumina in aqueous solution

Rakesh Kumar^a, Prabhakar Sharma^{a,*}, Abhay Kumar Aman^b, Rakesh Kumar Singh^b

^aSchool of Ecology and Environment Studies, Nalanda University, Rajgir, Bihar, India, Tel. +91 7033698509;

email: psharma@nalandauniv.edu.in (P. Sharma), Tel. +91 8873844901; email: rakumar.sees17@nalandauniv.edu.in (R. Kumar)

^bAryabhata Center for Nanoscience and Nanotechnology, School of Engineering and Technology, Aryabhata Knowledge University, Patna, Bihar, India, Tel. +91 767748990; email: abhayaman.aku@gmail.com (A.K. Aman), Tel. +91 81029155849;

email: rakeshsinghp@gmail.com (R.K. Singh)

Received 20 November 2019; Accepted 17 April 2020

ABSTRACT

Removal of fluoride is a desalination technology in which fluoride ions from aqueous solution are adsorbed on suitable adsorbent surfaces. In this study, adsorption potential was performed on both activated alumina (AA) and grinded activated alumina (GAA) by batch experiments for different contact time, pH, fluoride concentration, and adsorbent dose. Results indicated that adsorption occurred rapidly in the beginning, and equilibrium adsorption capacity was achieved as 23.73 and 28 mg g⁻¹ (i.e., mg of fluoride per g of alumina) in case of AA, whereas it was noted as 26.33 and 39 mg g⁻¹ for GAA for pH of 3.0 and fixed fluoride concentration of 75 and 100 mg L⁻¹, respectively in aqueous solution. Furthermore, adsorption isotherms were performed using three isotherm models in which the Freundlich model indicated a better fit (in the order of Freundlich > Langmuir > Dubinin–Radushkevich), showing heterogeneous nonlinear monolayer sorption. Consequently, pseudo-kinetics for fluoride adsorption on alumina particles for second-order ($R^2 > 0.98$) had better fit over the pseudo-first-order kinetic adsorption of fluoride. The exothermic behavior ($\Delta H^\circ = -58.78 \text{ J mol}^{-1}$) at solid–liquid interface delivered a decrease in fluoride adsorption with an increase in temperature of GAA. It has been noted that the adsorption of fluoride reduced in the presence of co-existing ions on AA and GAA, as the sorption capacity on adsorbent found in the order of $\text{CO}_3^{2-} > \text{PO}_4^{3-} > \text{SO}_4^{2-} > \text{NO}_3^- > \text{Cl}^-$. Results also revealed that the GAA could be a prospective adsorbent which can be regenerated as well as reused for the removal of fluoride ions from contaminated water.

Keywords: Activated alumina; Defluoridation; Adsorption mechanism; Kinetics; Batch experiment

1. Introduction

Fluorine is one of the richest (13th) essential components on the earth. In drinking water, fluoride is present in the form of fluoride ions (F⁻), which comes from natural or anthropogenic activities. Nowadays, the increase in anthropogenic activities threatens the environment and freshwater resources by releasing several organic and inorganic contaminants [1]. Inorganic pollutants have an ecological and toxicological impact on the aquatic

ecosystem, which impairs primary and secondary producers. The accessible limit for fluoride contamination used for drinking purposes is 1.5 mg L⁻¹, so about 260 million population are affected by fluoride contamination globally [2]. Fluoride is a major inorganic pollutant in India and across the globe including arsenic, nitrate, sulfate, pesticides, heavy metals, etc. and the fluoride contamination in groundwater leads to an adverse impact on human health and environment [3]. The conventional treatment method

* Corresponding author.

for fluoride contaminated water includes coagulation, flocculation, sedimentation, and filtration [1]. There are several approaches adopted for defluoridation of contaminated groundwater, that is, ion-exchange [4], membrane separation [5], adsorption [6], precipitation–coagulation [7], electrodialysis [8], and defluoridation using the electrolytic method [9]. Adsorption process has been reported as robust, eco-friendly, user-friendly and cost-effective in the order of adsorption > evaporation > ion-exchange > electrodialysis > reverse osmosis > precipitation > distillation [10].

Alumina (Al_2O_3) is a ceramic oxide having the extensive potential for water purification, as it possesses unique property having high surface area, surface acidity constants, and sorption capacity. Alumina has adsorption affinity as a result of the high point of zero charges, that is, $\text{pH}_{\text{pzc}} = 8.2$ for negatively charged fluoride ions [11]. Several studies had reported that adsorption of fluoride onto activated alumina is sensitive to pH. Therefore, the investigation of fluoride adsorption studied based on adjustment in pH can optimizes defluoridation. In that, the optimization of fluoride adsorption was reported maximum at $\text{pH} < 7.0$, while the minimum at $\text{pH} > 7.0$. Also, an electromagnetic force is dominant between activated alumina and fluoride ions at high pH [12].

The adsorption on alumina-based materials have been conducted at different physical and chemical conditions, that is, the function of varying pH, adsorbent dose, residence time, and initial fluoride concentration (C_f) [12,13]. Activated alumina (AA) has been widely used as an adsorbent for wastewater treatment because it has a high affinity for sorption of fluoride ions in the aqueous solution [14]. Considering AA as an adsorbent for defluoridation, the optimum removal of fluoride ions have resulted at a pH less than 6.0 in an aqueous solution [15]. Chinnakoti et al. [12] stated that nano γ -alumina had been synthesized using the combustion method, which was used as an adsorbent for defluoridation. The batch sorption experiment provided 96% of fluoride removal at pH 4.0 after reaching equilibrium within 2 h. Similarly, Mondal et al. [16] investigated that 97.5% fluoride was removed at pH 5.0 and temperature 313 K using aluminum impregnated coconut fibre. Bazrafshan et al. [13] investigated that 78.8% fluoride was removed at pH 5.0 with CuO nanoparticles in batch experiments. Lavecchia et al. [17] investigated that alumina containing bauxite could remove 38.5% fluoride at neutral pH and room temperature through batch and column adsorption trials. Ghorai and Pant [18] investigated that 69.5% of fluoride was removed at pH 7.0 by AA of 4–40 g L^{-1} in the solution, which hinted that adsorption onto AA could be sensitive towards pH, contact time, initial fluoride concentration, as well as its adsorbent dose. The adsorption of fluoride on alumina has been reported to decrease with increasing temperature, due to the mobility of fluoride ions from the solid phase to the bulk solution [16,19]. As groundwater contains various anions, such as chloride (Cl^-), phosphate (PO_4^{3-}), carbonate (CO_3^{2-}), nitrate (NO_3^-), sulfate (SO_4^{2-}), etc., the presence of anions can also influence the adsorption of fluoride on activated alumina [20].

The main objective of this study is to use reduced-size activated alumina for defluoridation as a function of pH, contact time, initial fluoride concentration, and adsorbent

dose through batch sorption experiments. It also aims to understand the sorption behavior of fluoride ions onto the adsorbent-water interfaces and the effect of co-existing ions and regeneration potential of fluoride contaminated water purification using different sizes of activated alumina.

2. Materials and methods

2.1. Characterization of activated alumina

The grinded activated alumina (GAA) was prepared from procured activated alumina (AA) (Merck, India) by mixing with acetone (Merck, India) for proper grinding on zirconium ball-mill (Retsch, Germany). The morphological and chemical characterization of AA and GAA were carried out using scanning electron microscopy (SEM, Carl Zeiss Microscopy, Zeiss, UK), Fourier transform infrared spectroscopy (FTIR, Perkin Elmer spectrum 400, Australia), X-ray diffractometer (Bruker, Germany), and nanoparticle tracking analyzer (NTA, nanosight NS300, Malvern Panalytical, UK) for particle size analysis. The zeta potential was determined by Zetasizer (NanoZ, Malvern Panalytical, UK) in DI water at varying pH of 3, 5, 9, and 11. The surface area analysis of AA and GAA were conducted with N_2 gas using Brunauer–Emmett–Teller (BET) analyzer (Micromeritics, MIC271002 REV B, 3Flex).

2.2. Stock solution preparation

Analytical grade chemicals procured from Merck, India were used for defluoridation studies. Fluoride stock solution was prepared using DI water for adsorption analysis at different pH (3, 7, and 11). The stock solution of fluoride was prepared using NaF (Merck, India) and DI water. The fluoride concentrations used in this study were 75 and 100 mg L^{-1} as the groundwater at the number of places in the world, including in India, maybe polluted with high fluoride content upto 100 mg L^{-1} [21]. The concentration of fluoride ions was estimated by UV-Vis spectrophotometer (Agilent Technology, AGILENT CARY100) at a wavelength of 274 nm. The alumina and fluoride solutions were mixed at a different initial fluoride concentration (C_f), contact time, and pH. The stock solution (1 mg L^{-1} concentration of GAA) was prepared using DI water for nanoparticle tracking. One-hundred milligram per liters of concentration of AA and GAA was made in millipore water for zeta potential analysis at varying pH of 3, 5, 9, and 11.

2.3. Batch sorption experiment

The adsorption behavior of fluoride with AA and GAA was studied by batch sorption method. The known quantity of fluoride with AA and GAA (25 mg) was placed in a 100 mL solution for varying pH conditions at room temperature (300 K) for 60 min duration. In addition, two sets of adsorption experiments were conducted at higher temperature (Table 1). The absorbance and their corresponding fluoride concentrations were measured using UV-Vis spectrophotometer as a function of time. The experimental parameters were also studied for the varying concentration of fluoride (75 and 100 mg L^{-1}), residence time (1–60 min), and pH (3, 7, and 11) as mentioned in Table 1. All the sorption

Table 1
Experimental conditions for adsorption of fluoride on AA and GAA in present study

| Experiment no. | Fluoride concentration C_F (mg L ⁻¹) | Adsorbent materials | Aqueous solution pH | Contact time (min) | Particles size (μm) | Surface area (BET) m ² g ⁻¹ | Temperature (K) | Equilibrium sorption (mg g ⁻¹) |
|----------------|--|---------------------|---------------------|--------------------|----------------------------------|---|-----------------|--|
| 1 | 75 | AA | 3 | 60 | 1–100 | 203.46 | 300 | 23.73 |
| 2 | 75 | AA | 7 | 60 | 1–100 | 203.46 | 300 | 20.33 |
| 3 | 75 | AA | 11 | 60 | 1–100 | 203.46 | 300 | 16.80 |
| 4 | 100 | AA | 3 | 60 | 1–100 | 203.46 | 300 | 28.09 |
| 5 | 100 | AA | 7 | 60 | 1–100 | 203.46 | 300 | 18.60 |
| 6 | 100 | AA | 11 | 60 | 1–100 | 203.46 | 300 | 16.84 |
| 7 | 75 | GAA | 3 | 60 | 0.177 | 216.66 | 300 | 26.42 |
| 8 | 75 | GAA | 7 | 60 | 0.177 | 216.66 | 300 | 23.66 |
| 9 | 75 | GAA | 11 | 60 | 0.177 | 216.66 | 300 | 16.64 |
| 10 | 100 | GAA | 3 | 60 | 0.177 | 216.66 | 300 | 38.71 |
| 11 | 100 | GAA | 7 | 60 | 0.177 | 216.66 | 300 | 25.93 |
| 12 | 100 | GAA | 11 | 60 | 0.177 | 216.66 | 300 | 18.84 |
| 13 | 100 | GAA | 3 | 60 | 0.177 | 216.66 | 318 | 35.13 |
| 14 | 100 | GAA | 3 | 60 | 0.177 | 216.66 | 338 | 26.84 |

trials were investigated in triplicate, and their mean value with their corresponding standard deviation are reported. The fluoride adsorption was performed as a function of contact time and initial concentrations of 75 and 100 mg L⁻¹ fluoride with variable pH 3, 7, and 11 of the aqueous solution. It was observed from the preliminary experiments that the batch analysis attained equilibrium at 60 min for 250 mg L⁻¹ of AA and GAA for both fluoride concentrations. The absorbance of fluoride ion was determined in DI water without and with the adsorbent in aqueous solution by UV-Vis spectrophotometer. The fluoride adsorption capacity, q_i (mg g⁻¹) onto the alumina at equilibrium was studied as:

$$q_i = \frac{(C_0 - C_t)V}{W} \quad (1)$$

where C_0 and C_t are initial and equilibrium concentrations of fluoride (mg L⁻¹), respectively, V represents the volume of aqueous solution (L), and W is equivalent to the weight of adsorbent (g).

The effect of co-existing ions was investigated by mixing 100 mg L⁻¹ concentration of anions obtained from each of these salts (NaCl, NaNO₃, Na₂SO₄, Na₃PO₄, and Na₂CO₃) with 100 mg L⁻¹ of initial fluoride concentration at pH 3 and an adsorbent dose of 250 mg L⁻¹ GAA and (as a similar to Mohan et al. [22]).

For regeneration study, GAA and AA were investigated for successive sorption–desorption processes (as a similar experiment to Chinnakoti et al. [12]). First, AA was saturated with an initial fluoride concentration of 100 mg L⁻¹ for 60 min. After reaching equilibrium, fluoride adsorbed AA was filtered and dried at 120°C. Then the dried sample of fluoride adsorbed AA was mixed with 0.1 M of NaOH solution and kept for 60 min after manually shaking for a few seconds. After cleaning the NaOH solution, the obtained sample was again applied for adsorption of

100 mg L⁻¹ concentration of fluoride at pH 3, and the equilibrium adsorbent capacity of AA was determined (cycle 1). The same experiment was repeated with the same adsorbent sample until the fifth cycle using 0.1 M NaOH. All the above steps were repeated for GAA.

2.4. Adsorption isotherms and kinetics

Langmuir model of sorption isotherm is valid for non-linear monolayer sorption on the homogeneous surface without interface among adsorbed particles. The uniform distribution of adsorption energies onto the homogeneous surface has been assumed with or without adsorbate movement [23]. On the other hand, Freundlich model of sorption isotherm are valid for nonlinear monolayer sorption on a heterogeneous surface having interaction among adsorbed molecules, and assumed heterogeneity in the distribution of adsorption energies onto the activated sites as well as with interaction among adsorbed particles [23]. The Langmuir isotherm is shown below [24]:

$$q_e = \frac{q_0 \beta C_e}{1 + \beta C_e} \quad (2)$$

$$\frac{1}{q_e} = \frac{1}{q_0 \beta C_e} + \frac{1}{q_0} \quad (3)$$

where q_e and q_0 are fluoride adsorption capacity at equilibrium as well as maximum amount of fluoride adsorption capacity (mg g⁻¹) respectively, C_e represents equilibrium amount of adsorbate (mg L⁻¹), and β is Langmuir equilibrium constant (L mg⁻¹).

The Langmuir isotherm has been validated using the separation parameter, R_L expressed by the following equation [25]:

$$R_L = \frac{1}{1 + \beta C_0} \quad (4)$$

The adsorption can be favorable for $0 < R_L < 1$, unfavorable for $R_L > 1$, and irreversible for $R_L = 0$.

The empirical equation for the Freundlich isotherm is given below [26]:

$$q_e = K_F C_e^{1/n} \quad (5)$$

$$\ln q_e = \left(\frac{1}{n}\right) \ln C_e + \ln K_F \quad (6)$$

where n represents Freundlich adsorption intensity and K_F is Freundlich adsorption capacity (mg g^{-1}).

Dubinin–Radushkevich adsorption isotherm explains the distribution of Gaussian energy onto heterogeneous adsorbent surfaces, which mainly distinguishes adsorption into physical or chemical sorption of metal ions in aqueous solution [27]. Dubinin–Radushkevich isotherm represented as [28]:

$$\ln q_e = \ln q_m - \beta_{\text{DR}} \varepsilon^2 \quad (7)$$

$$\varepsilon = RT \ln \left(1 + \frac{1}{C_e} \right) \quad (8)$$

where q_e and q_m are equilibrium and maximum adsorption capacity (mg g^{-1}), respectively, β_{DR} represents Dubinin–Radushkevich constant, ε is the adsorption potential, T represents temperature (K), and R is the universal gas constant ($8.314 \text{ J mol}^{-1} \text{ K}^{-1}$).

Adsorption kinetics explains the rate of fluoride uptake, in which residence time regulates the adsorption mechanism [29]. The kinetics of the adsorption process depends upon several factors, such as morphological properties of sorbent, sorbate concentration, and interactions of adsorbent and adsorbate [20]. Pseudo-first-order and pseudo-second-order kinetics are two commonly used mass transfer kinetics model. The pseudo-first-order model, also called the Lagergren model [30], explains the sorption kinetics as a factor of contact time. The equation for pseudo-first-order is given as follows:

$$\log(q_e - q_t) = \log(q_e) - \left(\frac{K_1}{2.303}\right)t \quad (9)$$

In pseudo-second-order kinetics, the rate for the chemical reaction has a direct relationship to active sites onto adsorbent, that is, the mechanism involved are the force of valance through exchange between adsorbent and adsorbate [31]. The general equation of the pseudo-second-order is:

$$\frac{t}{q_t} = \frac{1}{k_2 q_e^2} + \frac{1}{q_e} \quad (10)$$

where q_e and q_t are the fluoride adsorption capacity (mg g^{-1}) at equilibrium and at time t (minutes) respectively,

and k_1 and k_2 are the rate constant of pseudo-first and second-order kinetics.

2.5. Thermodynamic adsorption isotherm

The thermodynamic constants, such as standard entropy (ΔS°), free energy (ΔG°), enthalpy (ΔH°) determine the sorption feasibility of fluoride on GAA using equilibrium constant (K_c) and their corresponding temperature (T) as follows [12]:

$$\log(K_c) = \frac{\Delta S^\circ}{2.303R} - \left(\frac{\Delta H^\circ}{2.303R}\right)\frac{1}{T} \quad (11)$$

$$K_c = \frac{C_{\text{Ae}}}{C_e} \quad (12)$$

$$\Delta G = \Delta H^\circ - T\Delta S^\circ \quad (13)$$

where C_e and C_{Ae} are equilibrium concentration (mg L^{-1}) in the solution and on the adsorbent, respectively, and R is the universal gas constant ($8.314 \text{ J mol}^{-1} \text{ K}^{-1}$).

3. Results and discussion

3.1. Characterization of activated alumina and GAA

Scanning electron microscopic images depict the structural and morphological distribution of AA and GAA, as shown in Fig. 1. The primary shape of AA was almost spherical with high surface roughness, with particle size lies in the range of 1–100 μm (Fig. 1a). The shape of GAA was also spherical with an average diameter of 177 nm (Fig. 1b). However, GAA was distributed in the form of agglomerates. A similar structure of alumina nanoparticles has been reported earlier [32]. The specific surface area of AA and GAA was determined using BET as 203.46 and 216.66 $\text{m}^2 \text{ g}^{-1}$, respectively, and total area in the pores of AA and GAA was obtained as 99.76 and 104.50 $\text{cm}^2 \text{ g}^{-1}$, respectively. The measured surface area of GAA was not very high as compared to that of AA due to high agglomeration of GAA observed in Fig. 1b.

The FTIR spectral signature of AA and GAA have been reported in the literature based on both experimental and theoretical simulations about the presence of different functional groups. The spectrum characteristic of AA has been observed in the range of 700–4,000 cm^{-1} wavelength resulting in no sharp peak for AA (Fig. 2), which hints the presence of amorphous structure with disordered defect. Similar disordered defects were observed in the literature for alumina nanoparticles [33]. The signature of GAA indicated a crystallized structural phase, which differs from AA. The main peaks at 735 and 1,074 cm^{-1} wavelengths are assigned for Al–O stretching mode in a tetrahedron with symmetric bending of Al–O–H in both AA and GAA [33]. The band peak at 1,359 cm^{-1} , present in GAA, might have occurred due to the stretching vibrations of Al=O bond [34]. The occurrence of band peak at 1,647 cm^{-1} in AA and GAA might have been observed due to asymmetric

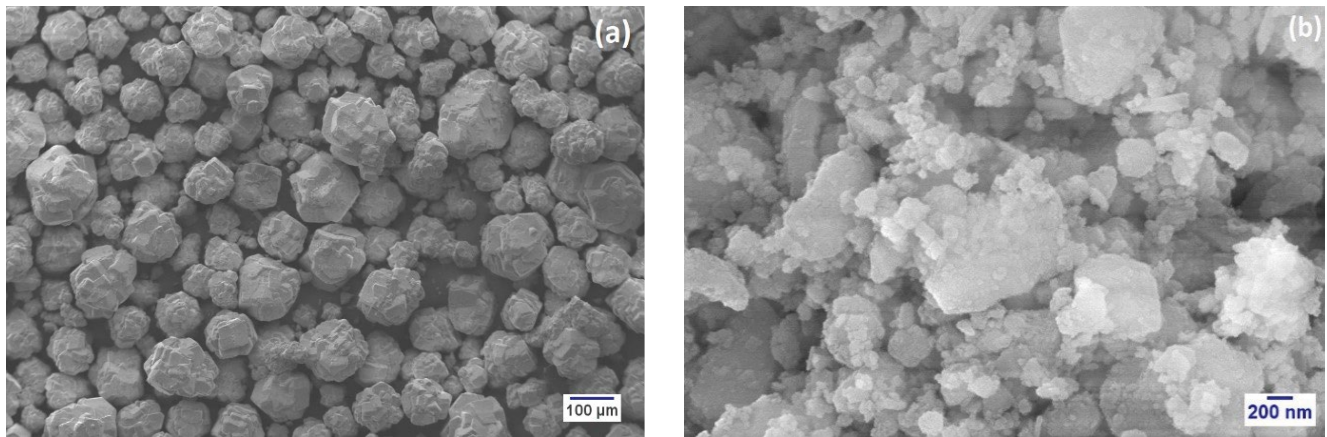


Fig. 1. Morphological analysis images for (a) AA and (b) GAA using SEM.

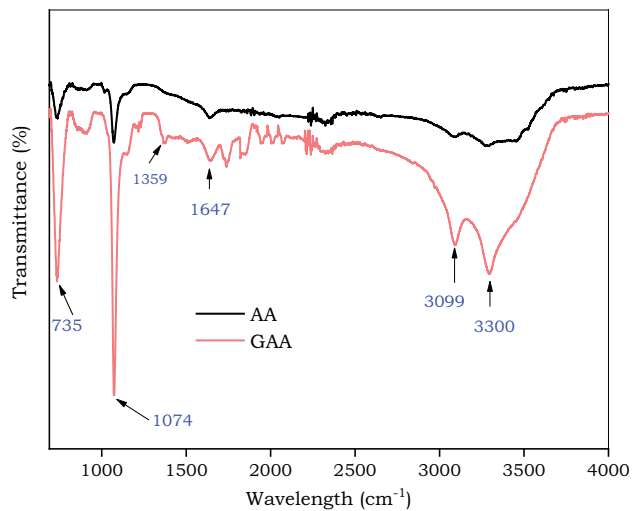


Fig. 2. FTIR of AA and GAA indicating functional groups mainly Al–O–H symmetric bending (at 735 and 1,074 cm^{-1}) as well as Al–O (at 1,359 cm^{-1}) and –OH (at 3,099 and 3,300 cm^{-1}) stretching vibrations.

stretching vibrations of $V_{\text{as}}(\text{COO})$ [35] and –OH bending [36]. In addition, the main peaks highlighted at 3,099 and 3,300 cm^{-1} were assigned for –OH stretching vibrations mode in AA and GAA [34].

The peaks in XRD pattern considerably supported the nano-sized Al_2O_3 and $\text{Al}(\text{OH})_3$ particles on the basis of ICDD (International Centre for Diffraction Data) database (COD-1101168- Al_2O_3 , COD-9012275- $\text{Al}(\text{OH})_3$) having an orthorhombic structure [37]. Nine reflections were observed at 2θ angles around 15° (020), 28° (021), 38° (130), 46° (131), 49° (002), 55° (151), 64° (132), 67° (171), and 72° (221) (Fig. 3). The lattice strain was found as 0.0031 and 0.0040 $\text{m}^2 \text{N}^{-1}$ by applying Debye–Scherrer formula for AA and GAA [38].

The zeta potential (ζ) analysis was performed to study the point of zero charges (PZC). At $\text{pH} < \text{pH}_{\text{PZC}}$, the adsorbent surface charge was positive, that is, it favors negatively charged adsorption and vice-versa [21]. At $\text{pH} 3$, ζ for AA and GAA were 13.9 ± 0.14 and 19.6 ± 0.7 mV, respectively.

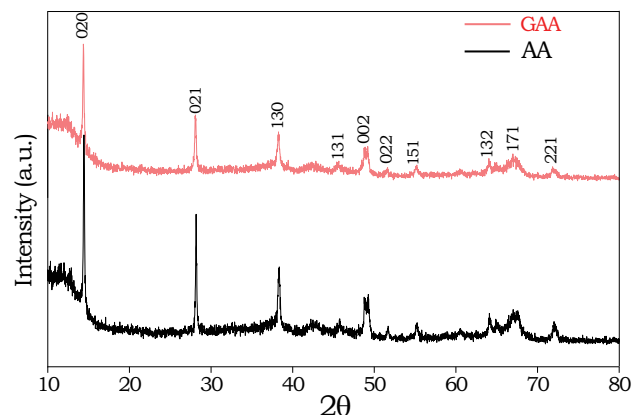


Fig. 3. XRD image of AA and GAA supporting the nano-sized Al_2O_3 and $\text{Al}(\text{OH})_3$ particles according to ICDD (International Centre for Diffraction Data) database (θ = Bragg's angle, radians).

However, ζ for AA were found as -10.9 ± 0.85 , -25.5 ± 0.9 , and -33.3 ± 2.6 mV at $\text{pH} 5, 9$, and 11 respectively. In addition, ζ values for GAA were -11.3 ± 3.9 , -13.1 ± 0.35 , and -31.0 ± 1.63 mV at $\text{pH} 5, 9$, and 11 respectively. Therefore, the electrostatic force between fluoride and adsorbent surfaces depends on interaction at varying pH . GAA had high adsorption capacity (mg g^{-1}) and fluoride removal percentage due to the existing interaction of electrostatic force, including van der Waals force [39].

3.2. Effect of contact time

Adsorption of fluoride on AA and GAA was depicted as a function of contact time in Figs. 4a and b with the fixed C_F of 75 mg L^{-1} and the adsorbent dose of 250 mg L^{-1} at $\text{pH} 3, 7$, and 11 . The concentration of fluoride in the batch experiments were obtained using Eq. (1). The contact time for adsorption was critical for achieving the equilibrium sorption, and the adsorption increased as a function of contact time from 1 to 60 min until the equilibrium sorption (Table 1). The q_t increased steadily upto 23.73 mg g^{-1} in case of AA (Fig. 4a), whereas it was achieved upto 26.42 mg g^{-1}

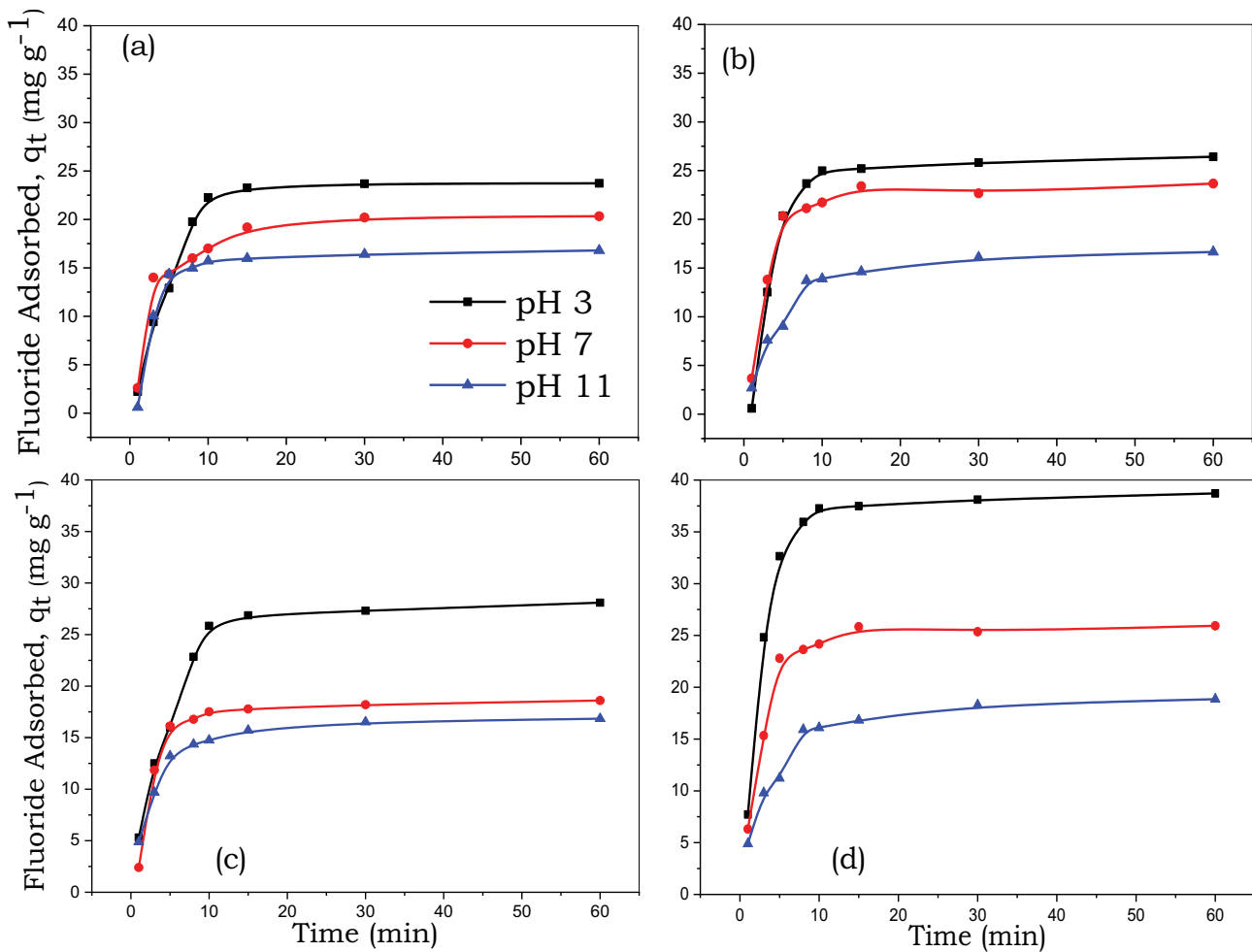


Fig. 4. Adsorption capacity of activated alumina (adsorbents) for fluoride at different pH for initial fluoride concentration: (a) $C_F = 75 \text{ mg L}^{-1}$ with AA, (b) $C_F = 75 \text{ mg L}^{-1}$ with GAA, (c) $C_F = 100 \text{ mg L}^{-1}$ with AA, and (d) $C_F = 100 \text{ mg L}^{-1}$ with GAA (Adsorbent dose = 250 mg L^{-1} and temperature = 300 K).

for GAA (Fig. 4b) for pH 3.0 condition. Similarly, the adsorption of fluoride ions on AA and GAA were studied for C_F of 100 mg L^{-1} and an adsorbent dose of 250 mg L^{-1} at pH 3, 7, and 11 (Figs. 4c and d). The q_t increased steadily upto 28.03 mg g^{-1} in case of AA (Fig. 4a), whereas it was upto 38.71 mg g^{-1} for GAA (Fig. 4b) at pH 3.0 condition. It was depicted that sorption of fluoride ions has direct correlation with contact time. Both AA and GAA possesses rapid uptake of fluoride initially and exhibited equilibrium later. A similar result for adsorption of fluoride on nano alumina nanoparticle was highlighted in previous literature [40]. Based on the preliminary experiments, equilibrium sorption was achieved within 60 min for the experimental conditions due to the availability of vacant sites over the alumina nanoparticle. So all batch experiments in this study were performed until 60 min only.

3.3. Effect of initial fluoride concentration and pH

For C_F of 75 and 100 mg L^{-1} , the adsorption capacity at equilibrium for AA and GAA was reported in Figs. 5a and b. The increase in adsorption of fluoride was due to the

greater availability of vacant sites on the positively charged surface of AA and GAA, as zeta potential value for AA was $13.9 \pm 0.14 \text{ mV}$, that is, less than ζ for GAA ($19.6 \pm 0.7 \text{ mV}$). A similar phenomenon is mentioned in the literature for adsorption of fluoride at nano alumina [40] and polystyrene sulfonate with alumina thin film [41]. Figs. 5a and b represent that maximum fluoride was adsorbed at pH 3.0 ($\text{pH} < \text{pH}_{\text{ZPC}}$) in both AA and GAA case, as their respective ζ were 13.9 ± 0.14 and $19.6 \pm 0.7 \text{ mV}$, respectively, which provided the availability of active vacant positive sites for negatively charged fluoride ions present in the aqueous solution. So, the adsorption of fluoride over alumina was strongly controlled by pH of an aqueous solution, which is also supported by Mondal et al. [16]. The adsorption at pH 3.0 was maximum, which was attributed due to $\text{pH} < \text{pH}_{\text{PZC}}$ having a maximum positive ζ , that is, adsorption of fluoride ions onto activated alumina surface was sensitive to pH. The chemistry of fluoride becomes more complicated by alumina as an adsorbent in the aqueous solution containing both fluoride ions and hydroxyl-aluminum complexes [11,42]. The mechanism for fluoride ion adsorption on alumina is explained below as the establishment of

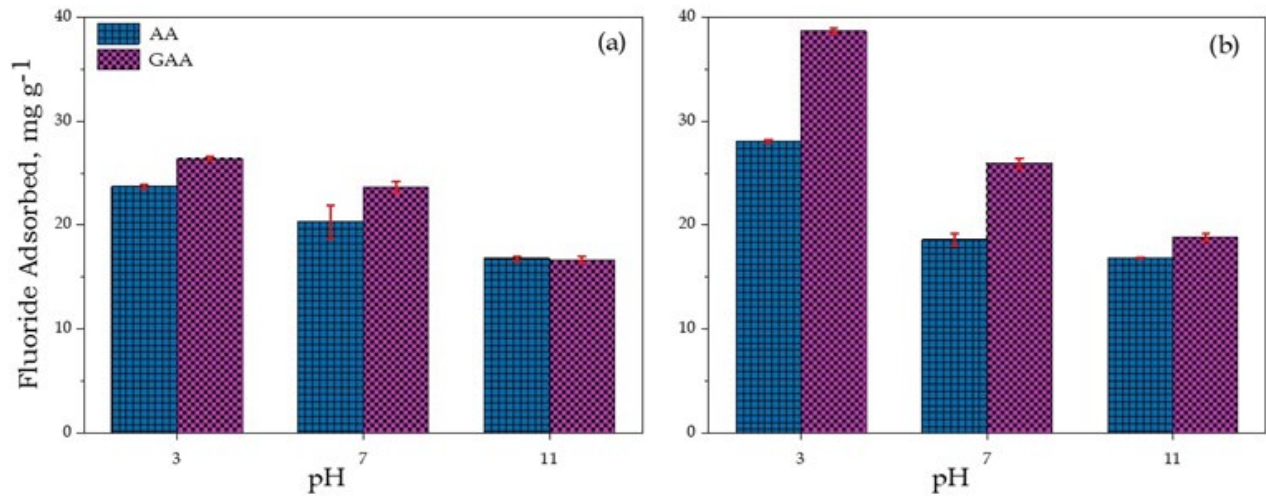
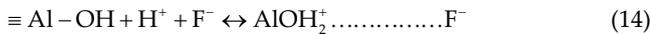


Fig. 5. Equilibrium adsorption capacity of AA and GAA for initial fluoride concentrations (a) $C_F = 75 \text{ mg L}^{-1}$ and (b) $C_F = 100 \text{ mg L}^{-1}$ at pH 3, 7, and 11. The error bar indicates standard deviation from three replicate experiments (adsorbent dose = 250 mg L^{-1} and temperature = 300 K , and residence time = 60 min).

inner surface complexity having surface hydroxyl sites, which involves ligand-exchange reaction [11,16,42]. The adsorption of fluoride occurs due to anion sites on alumina, such as aqua group ($-\text{Al}-\text{OH}_2^+$) and the hydroxy group ($-\text{Al}-\text{OH}$) [43].



In Fig. 5, AA and GAA having the specific surface area of 203.46 and $216.66 \text{ m}^2 \text{ g}^{-1}$ showed the maximum adsorption capacity of 28.09 and 38.71 mg g^{-1} , respectively (Table 1). The adsorption capacity of AA was less as compared to that of GAA, likely happened due to the reduction in total surface area for relatively big AA particles and higher negative zeta potential at pH 3, 7, and 11 as compared to their respective values of GAA. A similar result was observed for the specific surface area in case of unmodified alumina, and copper oxide coated alumina having surface area of 189.12 and $189.25 \text{ m}^2 \text{ g}^{-1}$ with the reported adsorption capacity of 2.23 and 7.77 mg g^{-1} , respectively [14].

The increase in C_F from 75 to 100 mg L^{-1} led to an increase in adsorption capacity of fluoride onto vacant sites of GAA and AA, respectively, at the fixed pH of 3.0 (Fig. 5). The mass transfer of fluoride on activated alumina was eased due to rapid diffusion of fluoride ions in aqueous solution to the active sites of activated alumina with an increase in initial fluoride concentration. The resistance during the mass exchange of fluoride ions at solid-liquid phase is overcome because of the driving force offered by higher fluoride concentration. It has been observed that hydroxyapatite and polypyrrole magnetic nanocomposite produced an increase in adsorption of fluoride ions at higher initial fluoride concentration [44,45].

3.4. Adsorption isotherms

Adsorption isotherm explains the diffusion of adsorbate, that is, fluoride ions into aqueous solution mixed with

adsorbents. The equilibrium adsorption was conducted to investigate the adsorption capacity of AA and GAA for fluoride, as the function of equilibrium fluoride concentration and sorption isotherm using Langmuir and Freundlich adsorption isotherms [46]. Various isotherm models have explained the adsorption of fluoride in equilibrium process, and the model are function of homogeneity of adsorbent surface, kind of coverage, and their interaction [47]. The equilibrium sorption study investigates the conditions for maximum removal of fluoride through activated alumina. It was reported that the complexity between solid and liquid phases gives the distribution of fluoride as a measure of equilibrium in the adsorption experiment [18].

For Langmuir, the plotting of $1/q_e$ vs. $1/C_e$ was investigated to define the coefficient of correlation, R^2 , q_m , and β (Table 2) for fluoride concentrations of 10 – 100 mg L^{-1} (absorbance was taken for $C_F = 10, 25, 50, 75,$ and 100 mg L^{-1} at 60 min only with adsorbents) for AA and GAA at varying pH solution using Eq. (3). R_L values are expressed between 0 and 1 (Table 2), confirming it's favorable for adsorption of fluoride on GAA and AA, using Eq. (4). In Freundlich isotherm, the plotting of $\ln(q_e)$ vs. $\ln(C_e)$ was investigated to determine the correlation coefficients, R^2 , K_F , and n (Table 2) for fluoride concentrations of 10 to 100 mg L^{-1} for AA and GAA at varying pH solution using Eq. (6). It is clear that fluoride adsorption in AA and GAA matched well with both Langmuir and Freundlich models, which explains the homogeneity as well as the heterogeneity of nonlinear monolayer sorption onto both adsorbents. According to Table 2, Freundlich adsorption intensity and reported n , has significant value as $n > 4$, which favor adsorption of fluoride on both adsorbent AA and GAA.

Dubinin–Radushkevich isotherm explains the distribution of Gaussian energy onto AA and GAA, using Eq. (7). The plotting of $\ln q_e$ vs. $1/C_e$ to determines R^2 , q_m' , and β_{DR} (Table 2) for fluoride adsorption. Therefore, the best-fit isotherm model, that is, Freundlich isotherm, was based on linear correlation coefficient (R^2) values at two different C_F . R^2

Table 2
Correlation coefficient, experimental and coefficient values of Langmuir, Freundlich, and Dubinin–Radushkevich isotherm for AA and GAA at pH 3, 7, and 11 (fluoride concentration = 10–100 mg L⁻¹, adsorbent dose = 250 mg L⁻¹, and residence time = 60 min)

| Particulars | Langmuir isotherm | | | | | Freundlich isotherm | | | | | Dubinin–Radushkevich | | | | | | | |
|-------------|-------------------|----------------|------|----------------|----------------|---------------------|----------------|------|----------------|----------------|----------------------|----------------|-------|------------------------|------------------------|-----------------|------------------------|-------------------------|
| | AA | | | | | AA | | | | | AA | | | | | | | |
| | R ² | q ₀ | β | R _L | R _L | R ² | q ₀ | β | R _L | R _L | R ² | K _F | n | R ² | q _m | β _{DR} | R ² | q _m |
| pH 3 | 0.87 | 27.64 | 0.31 | 0.24 | 0.85 | 0.85 | 36.62 | 0.37 | 0.21 | 0.99 | 2.86 | 4.31 | 0.92 | 22.19 | 5.8 × 10 ⁻⁶ | 0.81 | 22.41 | 9.02 × 10 ⁻⁷ |
| pH 7 | 0.81 | 19.3 | 0.35 | 0.22 | 0.84 | 22.26 | 0.39 | 0.20 | 0.98 | 2.3 | 4.52 | 0.95 | 17.30 | 4.6 × 10 ⁻⁵ | 0.90 | 20.35 | 3 × 10 ⁻⁶ | |
| pH 11 | 0.83 | 16.83 | 0.37 | 0.21 | 0.76 | 15.43 | 0.41 | 0.19 | 0.97 | 2.63 | 4.37 | 0.80 | 10.56 | 5 × 10 ⁻⁵ | 0.53 | 11.60 | 3.3 × 10 ⁻⁶ | |

value obtained from Freundlich isotherm was more significant than Langmuir isotherm and Dubinin–Radushkevich isotherm, based on the experimental data of fluoride adsorption. Besides, Freundlich and Dubinin–Radushkevich isotherms described the heterogeneity in sorption of fluoride ions; however, Langmuir isotherm explained sorption of fluoride ions on the homogeneous surface of AA and GAA. These results are supported by similar studies in the literature [48].

3.5. Adsorption kinetics

The adsorption kinetics was used to analyze the dynamics of the solute adsorption process. Hence, fluoride adsorption kinetics was also studied at different C_F of 75 and 100 mg L⁻¹ at fixed adsorbent dose of 250 mg L⁻¹ AA and GAA for 60 min at varying pH 3, 7, and 11. The pH of the fluoride solution is sensitive and influences adsorption of fluoride significantly. For pseudo-first-order kinetics, the value of k₁ and q_e (Table 3) were found from the analysis of the linearized form of pseudo-first-order Eq. (9), plotted as log(q_e - q_t) vs. t (Fig. 6). In addition to pseudo-first-order, pseudo-second-order kinetics is widely used as a model based on mass transfer dynamics. The value of k₂ and q_e were achieved from analysis of linear form of pseudo-second-order kinetic Eq. (10), plotted as t/q_t vs. t (Fig. 7). Table 4 depicted the correlation coefficient (R²), obtained from pseudo-second-order, which are higher than that of pseudo-first-order. Therefore, pseudo-second-order showed a significant relation between theoretical and experimental q_e and coefficient of correlation at two different C_F (Table 4). Similar results are mentioned in literature for pseudo-second-order as best fit for sorption process of fluoride [12,31].

3.6. Effect of temperature on fluoride adsorption and thermodynamic adsorption isotherm

The thermal energy can be increased at high temperature, resulting a increase in desorption of fluoride (i.e., 38.71–26.84 mg g⁻¹) for GAA from 300 to 338 K temperature. The tendency of fluoride ions for desorption is likely due to the exothermic nature of fluoride on GAA. A similar phenomenon have been observed in the literature for the adsorption of fluoride on alum sludge [19].

Table 5 depicts that the ΔH° and ΔS° can be evaluated from linear regression plotting of log(K_c) vs. 1/T using Eq. (11). The sorption of fluoride on GAA was obtained as a spontaneous process in nature showed by the negative value of ΔG° (-71,085.10 J mol⁻¹) at 300 K using Eq. (12). Besides, the positive value of ΔS° (236.75 J mol⁻¹K⁻¹) confirmed fluoride affinity toward activated alumina, which also suggests the increased randomness over the solid-solution interfaces. The negative ΔH° (-58.78 J mol⁻¹) supports the exothermic nature of the reaction. Similar results have been reported with adsorption of fluoride on aluminum impregnated coconut [16].

3.7. Effect of competing ions

Fig. 8 shows that the adsorption of fluoride ions onto AA and GAA has been suppressed by co-existence

Table 3

Kinetic constant and correlation coefficient for pseudo first order kinetics model for AA and GAA at pH 3, 7, and 11 and $C_F = 75$ and 100 mg L^{-1} (adsorbent dose = 250 mg L^{-1} and residence time = 60 min)

| Particulars | $C_F = 75 \text{ mg L}^{-1}$ | | | | | | $C_F = 100 \text{ mg L}^{-1}$ | | | | | |
|---------------------------------|------------------------------|--------|--------|--------|--------|--------|-------------------------------|--------|--------|---------|---------|---------|
| | AA | | | GAA | | | AA | | | GAA | | |
| | Exp. 1 | Exp. 2 | Exp. 3 | Exp. 7 | Exp. 8 | Exp. 9 | Exp. 4 | Exp. 5 | Exp. 6 | Exp. 10 | Exp. 11 | Exp. 12 |
| $k_1 \text{ (min}^{-1}\text{)}$ | 0.28 | 0.16 | 0.20 | 0.23 | 0.29 | 0.14 | 0.22 | 0.20 | 0.16 | 0.23 | 0.21 | 0.14 |
| R^2 | 0.96 | 0.97 | 0.74 | 0.75 | 0.49 | 0.92 | 0.81 | 0.74 | 0.92 | 0.74 | 0.73 | 0.92 |
| $q_{e,\text{exp}}$ | 1.37 | 1.30 | 1.22 | 1.37 | 1.35 | 1.14 | 1.44 | 1.26 | 1.22 | 1.58 | 1.41 | 1.27 |
| $q_{e,\text{cal}}$ | 1.53 | 1.18 | 1.06 | 1.42 | 1.37 | 1.22 | 1.47 | 1.06 | 1.03 | 1.40 | 1.21 | 1.14 |

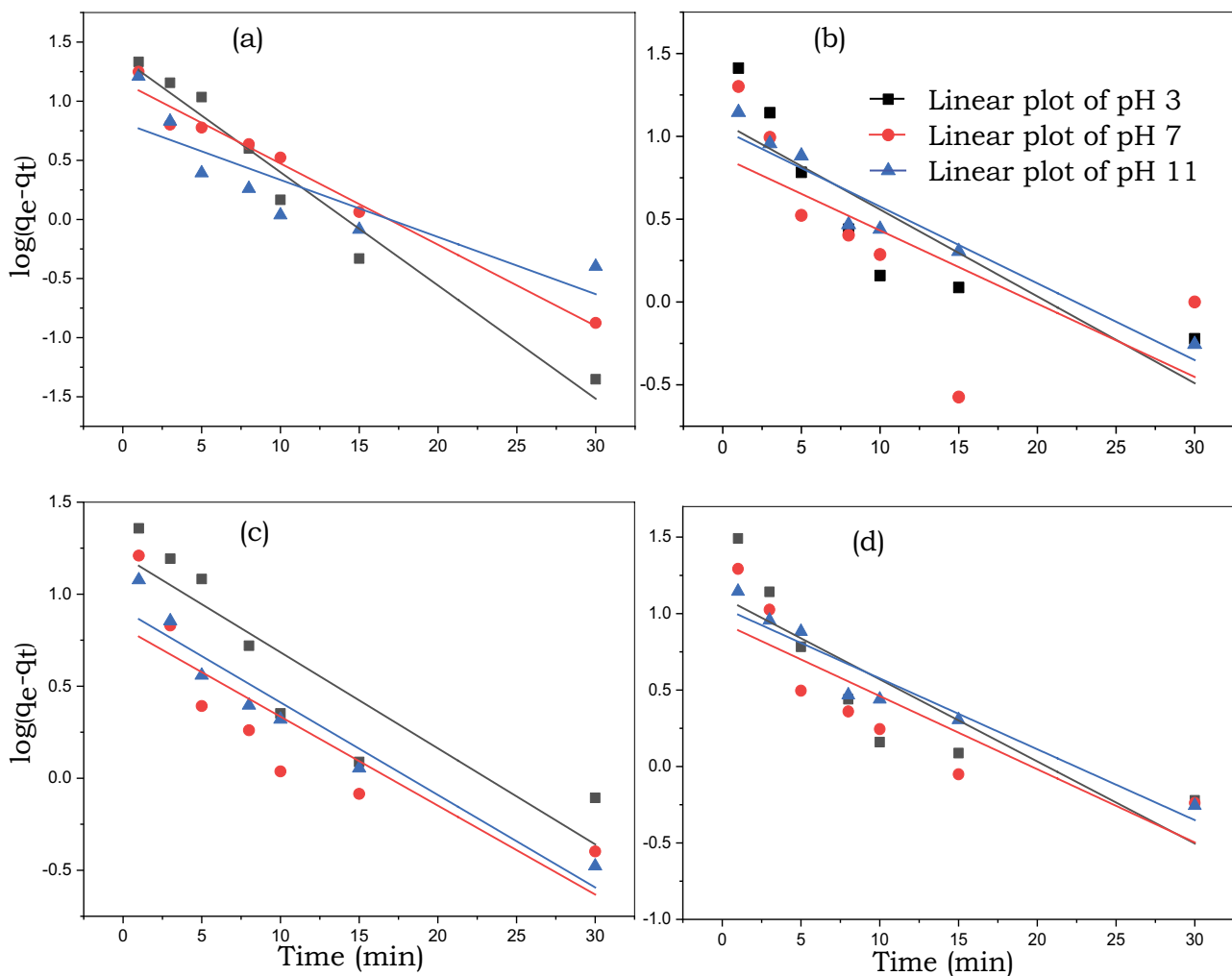


Fig. 6. Linear plot of pseudo-first-order kinetic for fluoride adsorption at different pH for initial fluoride concentration: (a) $C_F = 75 \text{ mg L}^{-1}$ with AA, (b) $C_F = 75 \text{ mg L}^{-1}$ with GAA, (c) $C_F = 100 \text{ mg L}^{-1}$ with AA, and (d) $C_F = 100 \text{ mg L}^{-1}$ with GAA (adsorbent dose = 250 mg L^{-1} , temperature = 300 K, and residence time = 60 min).

of Cl^- , PO_4^{3-} , CO_3^{2-} , NO_3^- , and SO_4^{2-} ions in the solution. The sorption capacity decreases with the presence of anions, such as CO_3^{2-} (30.0 mg g^{-1}), PO_4^{3-} (26.4 mg g^{-1}), SO_4^{2-} (20.8 mg g^{-1}), NO_3^- (19.6 mg g^{-1}), Cl^- (16.8 mg g^{-1}) for GAA

and CO_3^{2-} (28.09 mg g^{-1}), PO_4^{3-} (26.4 mg g^{-1}), SO_4^{2-} (19.2 mg g^{-1}), NO_3^- (15.2 mg g^{-1}), Cl^- (14.0 mg g^{-1}) for AA adsorbent. Similar results were observed for the removal of fluoride using nano-alumina [40]. Here, the carbonate, sulfate, and

Table 4
Kinetic constant and correlation coefficient for pseudo-second-order kinetics model for AA and GAA at pH 3, 7, and 11 and $C_F = 75$ and 100 mg L^{-1} (adsorbent dose = 250 mg L^{-1} and residence time = 60 min)

| Particulars | $C_F = 75 \text{ mg L}^{-1}$ | | | | | | $C_F = 100 \text{ mg L}^{-1}$ | | | | | |
|---|------------------------------|--------|--------|--------|--------|--------|-------------------------------|--------|--------|---------|---------|---------|
| | AA | | | GAA | | | AA | | | GAA | | |
| | Exp. 1 | Exp. 2 | Exp. 3 | Exp. 7 | Exp. 8 | Exp. 9 | Exp. 4 | Exp. 5 | Exp. 6 | Exp. 10 | Exp. 11 | Exp. 12 |
| $k_2 \text{ (g mg}^{-1} \text{ min}^{-1}\text{)}$ | 0.013 | 0.023 | 0.044 | 0.020 | 0.031 | 0.056 | 0.010 | 0.020 | 0.028 | 0.014 | 0.023 | 0.017 |
| R^2 | 0.994 | 0.999 | 1.0 | 0.998 | 0.999 | 0.998 | 0.996 | 0.990 | 0.999 | 0.997 | 0.998 | 0.999 |
| $q_{e,exp}$ | 23.73 | 20.33 | 16.8 | 26.42 | 23.66 | 16.64 | 28.09 | 18.6 | 16.84 | 38.71 | 25.93 | 18.84 |
| $q_{e,cal}$ | 25.29 | 21.11 | 17.17 | 27.33 | 24.14 | 17.68 | 29.95 | 19.60 | 17.46 | 40.14 | 26.77 | 19.81 |

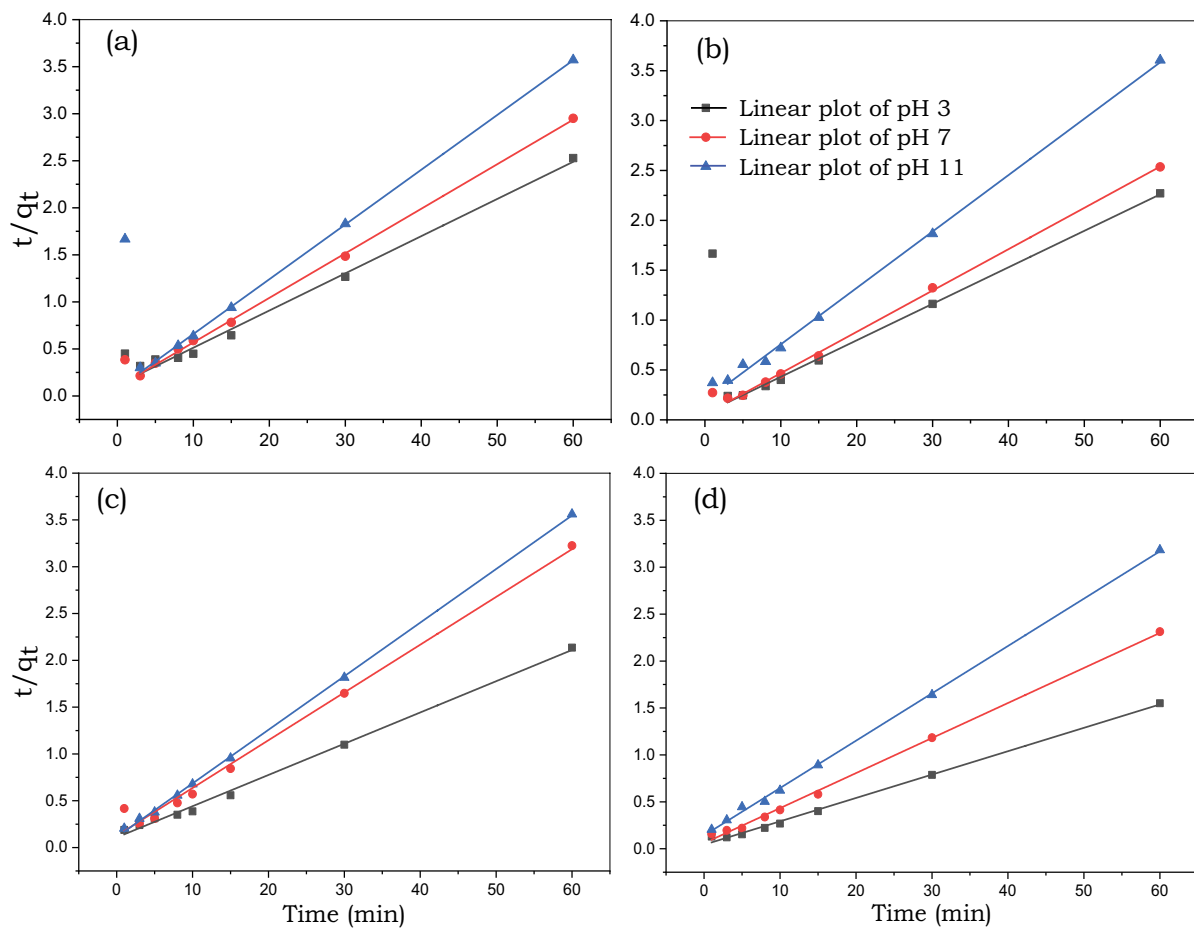


Fig. 7. Linear plot of pseudo-second-order kinetic for fluoride adsorption at different pH for initial fluoride concentration: (a) $C_F = 75 \text{ mg L}^{-1}$ with AA, (b) $C_F = 75 \text{ mg L}^{-1}$ with GAA, (c) $C_F = 100 \text{ mg L}^{-1}$ with AA, and (d) $C_F = 100 \text{ mg L}^{-1}$ with GAA (adsorbent dose = 250 mg L^{-1} , temperature = 300 K, and residence time = 60 min).

Table 5
Thermodynamic analysis of grinded activated alumina (GAA) ($C_F = 100 \text{ mg L}^{-1}$, adsorbent dose = 250 mg L^{-1} , pH = 3, and residence time = 60 min)

| $\Delta S^\circ \text{ (J mol}^{-1}\text{K}^{-1}\text{)}$ | $\Delta H^\circ \text{ (J mol}^{-1}\text{)}$ | $\Delta G^\circ \text{ (J mol}^{-1}\text{)}$ | | |
|---|--|--|-----------|-----------|
| | | 300 K | 318 K | 338 K |
| 236.75 | -58.78 | -71,085.1 | -75,346.7 | -80,081.8 |

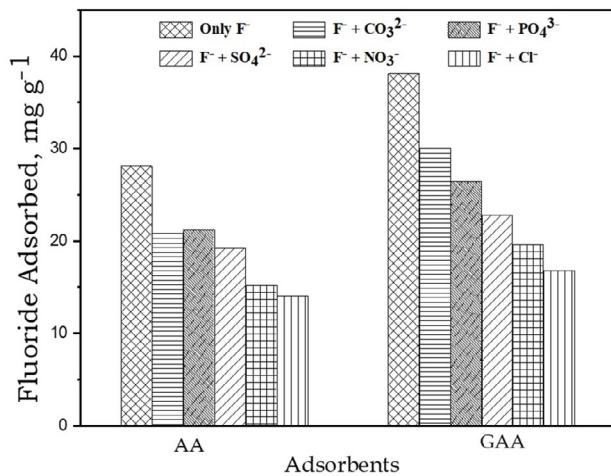


Fig. 8. Influence of coexisting ions on fluoride sorption on GAA and AA (temperature = 300 K, pH = 3, residence time = 60 min, adsorbent dose = 250 mg L⁻¹, and C_F = 100 mg L⁻¹).

phosphate are inner-spherically sorbing anions, which have shown high adsorption of fluoride than the outer spherically sorbing ions (chloride and nitrate ions).

3.8. Reusability of adsorbent GAA

Desorption of adsorbate mainly leads to the sustainability of the adsorbent. The adsorption capacity showed that the significant regeneration of adsorbent can occur in the first three cycles; after that, no significant change was observed in fourth and fifth cycles for both GAA and AA (Fig. 9). The adsorption capacity of AA and GAA (i.e., without NaOH) were about 28 and 38 mg g⁻¹ respectively, which reduced after regeneration, in first three cycles and reached up to 34 mg g⁻¹ for GAA and 20 mg g⁻¹ for AA in the fifth cycle (Fig. 9). The desorption mechanism offers fluoride regeneration likely due to electrostatic force and ion exchange, where OH⁻ might have removed the fluoride ions attached with AA and GAA. The adsorbed molecule escapes the surface when it acquires high or equal energy to the adsorption energy [19].

The reusability of activated alumina adsorbent makes the fluoride sorption cost-effective. So, the outcomes in this study establish that activated alumina can be efficient and appropriate adsorbent for sorption of fluoride ions. The adsorption of fluoride on alumina can also be considered a sophisticated and straightforward process for wastewater treatment.

4. Conclusions

The adsorption of fluoride by AA and GAA established as a function of solution pH, contact time as well as initial fluoride concentrations. Therefore, the driving force for the abstraction of fluoride was the concentration gradient of fluoride due to mass transfer at aqueous-solid phases. Freundlich isotherm preferred as a best fit model for sorption equilibrium analysis among Freundlich, Langmuir, and Dubinin–Radushkevich adsorption isotherm models.

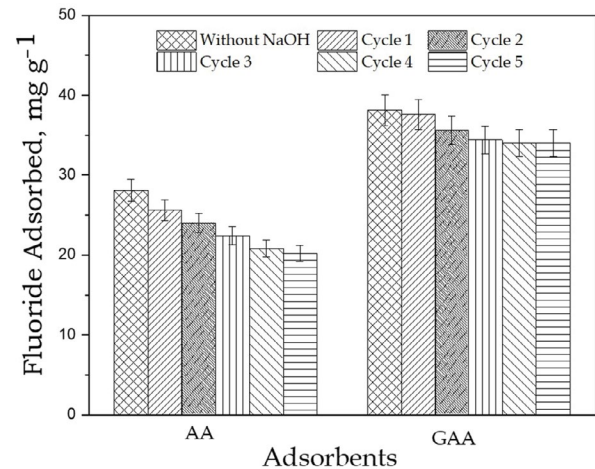


Fig. 9. Regeneration cycles of AA and GAA using 0.1 M NaOH (C_F = 100 mg L⁻¹, adsorbent dose = 250 mg L⁻¹, and pH = 3). “Without NaOH” denotes the original experiment number 4 and 10 for AA and GAA respectively as listed in Table 1. The successive reuse of adsorbent AA and GAA obtained after exp. 4 and 10 with 0.1 M NaOH are denoted by cycles 1, 2, 3, 4, and 5. The error bar indicates standard deviation from three replicate experiments.

In addition, the pseudo-second-order kinetic was better suited over the pseudo-first-order kinetics experimental data of fluoride adsorption in this study. As pH is significant for adsorption capacity, the fluoride removal was depicted maximum at pH 3.0, while fluoride adsorption onto AA and GAA decreased at pH 7.0 and above as a result of less availability of vacant positive sites on activated alumina surfaces. As C_F increases from 75 to 100 mg L⁻¹, fluoride adsorbed onto alumina surface leads to an increase in adsorption capacity. It has also been observed that adsorption of fluoride reduced with increasing temperature. Based on fluoride removal using AA and GAA, GAA has high adsorption capacity to describe the wastewater treatment adequately. In the presence of competing anions, it has been noted that the adsorption of fluoride has reduced on AA and GAA, as the sorption capacity on adsorbent are presented in the order of CO₃²⁻ > PO₄³⁻ > SO₄²⁻ > NO₃⁻ > Cl⁻. The sustainability of adsorbent demonstrated that GAA has the potential to be regenerated and reused for defluoridation. The study on fluoride ion removal in batch sorption experiments was found robust using GAA so it could be a favorable material for optimal removal of fluoride ions from wastewater. Further, adsorption of fluoride is a sophisticated and cheap technology that requires suitable design and operational parameters for wastewater treatment. Finally, the adsorption model using size reduced activated alumina enable an optimum removal of fluoride as a function of contact time and pH, including the different concentrations of fluoride ions in an aqueous solution of alumina and fluoride.

Acknowledgments

We are grateful to Dr. Manoranjan Kar and his team, IIT Patna, Patna for helping in the zeta potential, FTIR, particle size analysis. Along with, we are sincerely thankful to Prof.

Vivek Polshettiwar, Department of Chemical Sciences, Tata Institute of Fundamental Research (TIFR), Mumbai for helping us in surface area analysis of activated alumina.

References

- [1] J.A. Camargo, Á. Alonso, Ecological and toxicological effects of inorganic nitrogen pollution in aquatic ecosystems: a global assessment, *Environ. Int.*, 32 (2006) 831–849.
- [2] WHO, Surveillance and Control of Community Supplies, Guidelines for Drinking-Water Quality, World Health Organization, Geneva, 1997.
- [3] C.F. Harvey, C.H. Swartz, A.B.M. Badruzzaman, N. Keon-Blute, W. Yu, M.A. Ali, J. Jay, R. Beckie, V. Niedan, D. Brabander, Groundwater arsenic contamination on the Ganges Delta: biogeochemistry, hydrology, human perturbations, and human suffering on a large scale, *C. R. Geosci.*, 337 (2005) 285–296.
- [4] G. Singh, B. Kumar, P. Sen, J. Majumdar, Removal of fluoride from spent pot liner leachate using ion exchange, *Water Environ. Res.*, 71 (1999) 36–42.
- [5] Z. Amor, B. Bariou, N. Mameri, M. Taky, S. Nicolas, A. Elmidaoui, Fluoride removal from brackish water by electrodialysis, *Desalination*, 133 (2001) 215–223.
- [6] A. Raichur, M.J. Basu, Adsorption of fluoride onto mixed rare earth oxides, *Sep. Purif. Technol.*, 24 (2001) 121–127.
- [7] E.J. Reardon, Y. Wang, A limestone reactor for fluoride removal from wastewaters, *Environ. Sci. Technol.*, 34 (2000) 3247–3253.
- [8] M. Hichour, F. Persin, J. Sandeaux, J. Molenat, C. Gavach, Water defluoridation by Donnan dialysis and electrodialysis, *Water Sci.*, 12 (1999) 671–686.
- [9] N. Mameri, H. Lounici, D. Belhocine, H. Grib, D. Piron, Y. Yahiat, Defluoridation of Sahara water by small plant electrocoagulation using bipolar aluminium electrodes, *Sep. Purif. Technol.*, 24 (2001) 113–119.
- [10] I. Ali, New generation adsorbents for water treatment, *Chem. Rev.*, 112 (2012) 5073–5091.
- [11] A. Salifu, Fluoride Removal from Groundwater by Adsorption Technology, CRC Press, Netherlands, 2017.
- [12] P. Chinnakoti, A.L. Chunduri, R.K. Vankayala, S. Patnaik, V. Kamiseti, Enhanced fluoride adsorption by nano crystalline γ -alumina: adsorption kinetics, isotherm modeling and thermodynamic studies, *Appl. Water Sci.*, 7 (2017) 2413–2423.
- [13] E. Bazrafshan, D. Balarak, A.H. Panahi, H. Kamani, A.H. Mahvi, Fluoride removal from aqueous solutions by cupric oxide nanoparticles, *Fluoride*, 49 (2016) 233–244.
- [14] A. Bansawal, P. Pillewan, R.B. Biniwale, S.S. Rayalu, Copper oxide incorporated mesoporous alumina for defluoridation of drinking water, *Microporous Mesoporous Mater.*, 129 (2010) 54–61.
- [15] C. Martyn, C. Osmond, J. Edwardson, D. Barker, E. Harris, R. Lacey, Geographical relation between Alzheimer's disease and aluminium in drinking water, *Lancet*, 333 (1989) 59–62.
- [16] N.K. Mondal, R. Bhaumik, J.K. Datta, Removal of fluoride by aluminum impregnated coconut fiber from synthetic fluoride solution and natural water, *Alex. Eng. J.*, 54 (2015) 1273–1284.
- [17] R. Lavecchia, F. Medici, L. Piga, G. Rinaldi, A. Zuorro, Fluoride removal from water by adsorption on a high alumina content bauxite, *Chem. Eng.*, 26 (2012) 225–230.
- [18] S. Ghorai, K. Pant, Equilibrium, kinetics and breakthrough studies for adsorption of fluoride on activated alumina, *Sep. Purif. Technol.*, 42 (2005) 265–271.
- [19] N.A.A. Nazria, R.S. Azisa, H.C. Man, A.H. Shaari, N.M. Saiden, I. Ismail, Equilibrium studies and dynamic behaviour of cadmium adsorption by magnetite nanoparticles extracted from mill scales waste, *Desal. Water Treat.*, 171 (2019) 115–131.
- [20] S.M. Maliyekkal, S. Shukla, L. Philip, I.M. Nambi, Enhanced fluoride removal from drinking water by magnesia-amended activated alumina granules, *Chem. Eng. J.*, 140 (2008) 183–192.
- [21] D. Mohan, R. Sharma, V.K. Singh, P. Steele, C.U. Pittman Jr, Fluoride removal from water using bio-char, a green waste, low-cost adsorbent: equilibrium uptake and sorption dynamics modeling, *Ind. Eng. Chem. Res.*, 51 (2012) 900–914.
- [22] M. Aslam, S. Rais, M. Alam, A. Pugazhendi, Adsorption of Hg(II) from aqueous solution using *Adulsa (Justicia adhatoda)* leaves powder: kinetic and equilibrium studies, *J. Chem.*, (2013), doi: 10.1155/2013/174807.
- [23] I. Langmuir, The constitution and fundamental properties of solids and liquids. Part I. Solids, *J. Am. Chem. Soc.*, 38 (1916) 2221–2295.
- [24] K.R. Hall, L.C. Eagleton, A. Acrivos, T. Vermeulen, Pore- and solid-diffusion kinetics in fixed-bed adsorption under constant-pattern conditions, *Ind. Eng. Chem. Fundam.*, 5 (1966) 212–223.
- [25] H. Freundlich, Over the adsorption in solution, *J. Phys. Chem.*, 57 (1906) 1100–1107.
- [26] C. Travis, E.L. Etnier, A survey of sorption relationships for reactive solutes in soil, *J. Environ. Qual.*, 10 (1981) 8–17.
- [27] D.N. Misra, Adsorption on heterogeneous surfaces: a Dubinin–Radushkevich equation, *Surf. Sci.*, 18 (1969) 367–372.
- [28] V. Karthik, K. Saravanan, N. Sivarajasekar, N. Suriyanarayanan, Utilization of biomass from *Trichoderma harzianum* for the adsorption of reactive red dye, *Ecol. Environ. Conserv.*, 22 (2016) S435–S440.
- [29] S. Lagergren, Zur theorie der sogenannten adsorption gelöster stoffe, *Kungl. Sven. Vetenskapsakad. Handl.*, 24 (1898) 1–39.
- [30] N. Sivarajasekar, T. Paramasivan, S. Muthusaravanan, P. Muthukumar, S. Sivamani, Defluoridation of water using adsorbents—a concise review, *J. Environ. Biotechnol. Res.*, 6 (2017) 186–198.
- [31] M. Zawrah, R. Khattab, L. Girgis, H. El Daidamony, R.E.A. Aziz, Stability and electrical conductivity of water-base Al_2O_3 nanofluids for different applications, *HBRC J.*, 12 (2016) 227–234.
- [32] K. Djebaili, Z. Mekhalif, A. Boumaza, A. Djelloul, XPS, FTIR, EDX, and XRD analysis of Al_2O_3 scales grown on PM2000 alloy, *J. Spectrosc.*, (2015), doi: 10.1155/2015/868109.
- [33] D.C. Vasconcelos, E.H. Nunes, W.L. Vasconcelos, AES and FTIR characterization of sol–gel alumina films, *J. Non-Cryst. Solids*, 358 (2012) 1374–1379.
- [34] S.A. Hosseini, A. Niaei, D. Salari, Production of $\gamma\text{-Al}_2\text{O}_3$ from Kaolin, *Open J. Phys. Chem.*, 1 (2011) 23–27.
- [35] S. Gupta, P.C. Ramamurthy, G. Madras, Synthesis and characterization of flexible epoxy nanocomposites reinforced with amine functionalized alumina nanoparticles: a potential encapsulant for organic devices, *Polym. Chem.*, 2 (2011) 221–228.
- [36] Y. Piña-Pérez, O. Aguilar-Martínez, S. Oros-Ruiz, R. Gómez, F. Tzompantzi, Commercial aluminum oxides with different crystalline structures efficient for the mineralization of phenolic pollutants, *J. Photochem. Photobiol., A*, 353 (2018) 409–415.
- [37] P. Scherrer, Bestimmung der Inneren Struktur und der Größe von Kolloidteilchen Mittels Röntgenstrahlen, In: *Kolloidchemie Ein Lehrbuch, Chemische Technologie in Einzeldarstellungen*, Springer, Berlin, Heidelberg, 1912, pp. 387–409.
- [38] J. Qiao, Z. Cui, Y. Sun, Q. Hu, X. Guan, Simultaneous removal of arsenate and fluoride from water by Al-Fe (hydr) oxides, *Front. Environ. Sci. Eng.*, 8 (2014) 169–179.
- [39] E. Kumar, A. Bhatnagar, U. Kumar, M. Sillanpää, Defluoridation from aqueous solutions by nano-alumina: characterization and sorption studies, *J. Hazard. Mater.*, 186 (2011) 1042–1049.
- [40] N. Gupta, V. Gupta, A. Singh, R. Singh, Defluoridation of groundwater using low cost adsorbent like bagasse dust, aluminium treated bagasse flyash, bone powder and shell powder, *Bonfring Int. J. Ind. Eng. Manage. Sci.*, 4 (2014) 72–75.
- [41] T.C. Prathna, A.M. Raichur, Fluoride removal from aqueous solutions using poly(styrene sulfonate)/nanoalumina multilayer thin films, *Global Challenges*, 2 (2018) 1700064.
- [42] M. Mourabet, A. El Rhilassi, H. El Boujaady, M. Bennani-Ziatni, R. El Hamri, A. Taitai, Removal of fluoride from aqueous solution by adsorption on hydroxyapatite (HAp) using response surface methodology, *J. Saudi Chem. Soc.*, 19 (2015) 603–615.
- [43] U.O. Aigbe, R.B. Onyancha, K.E. Ukhurebor, K.O. Obodo, Removal of fluoride ions using a polypyrrole magnetic nanocomposite influenced by a rotating magnetic field, *RSC Adv.*, 10 (2020) 3883–3883.

- [44] J. Singh, P. Singh, A. Singh, Fluoride ions vs. removal technologies: a study, *Arabian J. Chem.*, 9 (2016) 815–824.
- [45] W.W. Choi, K.Y. Chen, The removal of fluoride from waters by adsorption, *J. Am. Water Works Assoc.*, 71 (1979) 562–570.
- [46] G.E.J. Poinern, M.K. Ghosh, Y.J. Ng, T.B. Issa, S. Anand, P. Singh, Defluoridation behavior of nanostructured hydroxyapatite synthesized through an ultrasonic and microwave combined technique, *J. Hazard. Mater.*, 185 (2011) 29–37.
- [47] Q. Liu, L. Zhang, B. Yang, R. Huang, Removal of fluoride from aqueous solution using Zr(IV) immobilized cross-linked chitosan, *Int. J. Biol. Macromol.*, 77 (2015) 15–23.
- [48] G. Tomar, A. Thareja, S. Sarkar, Enhanced fluoride removal by hydroxyapatite-modified activated alumina, *Int. J. Environ. Sci. Technol.*, 12 (2015) 2809–2818.